

# **Experimental investigation of capillary thermodynamics in fibrous materials**

Research project 1 – 085851

Michael Ushakov  
Advisor: Alexandros Terzis

## Abstract

Plasma treatment of paper-based materials is already in high use in different big industries, while all the effects of haven't been studied yet. The following project was focused on hydrogen and oxygen plasma treatment of a paper-based material specifically on the dynamic and thermodynamic effects of it. Hydrogen and oxygen plasma treatment was performed on a pure cellulose paper samples. Then the samples were exposed to a bath of water and went wet. The effects were caught using a high-speed IR camera and then post-processed via the computer. Our main conclusions were that oxygen and hydrogen plasma treatment affect both dynamics and thermodynamic of the imbibition process. Also, we noticed a change in the contact angle of the surface with water. Oxygen plasma treatment makes the surface more hydrophilic and increases the wettability of the surface while hydrogen plasma treatment does the opposite effect.

## Table of Contents

<b>Abstract .....</b>	<b>1</b>
<b>Table of figures.....</b>	<b>3</b>
<b>Scientific Background .....</b>	<b>4</b>
<b>Capillary pressure and wicking dynamics.....</b>	<b>4</b>
<b>Multi component surface energy theories .....</b>	<b>6</b>
Fowkes approach [11] .....	6
Owens and Wendt model[12].....	7
van Oss model [13].....	7
<b>Capillary thermodynamics in fibrous materials .....</b>	<b>8</b>
<b>Objective and goals.....</b>	<b>9</b>
<b>Materials and Methods .....</b>	<b>10</b>
<b>Experimental system.....</b>	<b>10</b>
<b>Sample material.....</b>	<b>11</b>
<b>Plasma treatment .....</b>	<b>13</b>
<b>FTIR spectroscopy analysis .....</b>	<b>16</b>
<b>Post-processing Program .....</b>	<b>18</b>
<b>Results and Discussion .....</b>	<b>19</b>
<b>Dynamic effect of plasma treatment.....</b>	<b>19</b>
<b>Thermodynamic effect of plasma treatment .....</b>	<b>20</b>
<b>Contact angle estimation .....</b>	<b>22</b>
<b>Conclusion .....</b>	<b>25</b>
<b>Bibliography.....</b>	<b>26</b>

## Table of figures

Figure 1: contact angle representation .....	5
Figure 2: heat release demonstration in a paper sample filled with water from [26] .....	9
Figure 3: Experimental setup from [25].....	10
Figure 4: Chemical structure of cellulose .....	11
Figure 5: XRD analysis for paper sample.....	11
Figure 6: SEM top view pictures for the untreated paper sample.....	12
Figure 7: SEM side view pictures for the untreated paper sample .....	12
Figure 8: Plasma treatment system .....	13
Figure 9: Plasma treatment process for Ambient air , Hydrogen and Oxygen plasmas .....	14
Figure 10: Paper samples that are used in the experiment.....	14
Figure 11: Paper sample putted in the plasma treatment machine.....	15
Figure 12: An example from [28] to an IR spectrum for a cellulose membrane .....	16
Figure 13: IR spectrum for 3 different treated paper samples (untreated, oxygen treated, hydrogen treated) .....	17
Figure 14: imbibition height vs time. for different types of plasma surface treatment for a 3mm paper sample .....	19
Figure 15: imbibition height vs time. for different types of plasma surface treatment for a 6mm paper sample .....	19
Figure 16: Temperature rise vs. Imbibition velocity for 3mm oxygen plasma treated and untreated paper.....	20
Figure 17: Temperature rise vs. Imbibition velocity for 6mm oxygen and hydrogen plasma treated and untreated paper .....	21
Figure 18: Temperature rise vs. Imbibition height for 6mm oxygen and hydrogen plasma treated and untreated paper .....	22
Figure 19: z <sup>2</sup> as a function of t with the approximated slope for an experiment of pentane with untreated paper sample .....	23
Figure 20: A schematic representation of the molecular interactions between cellulose and imbibed water from [26] .....	24

## Scientific Background

Paper-based materials are widely used in all the big industries that affect our everyday life directly. As example, microfluidic paper-based materials are used as medical diagnostic tools and for laboratory procedures [1], [2]. Those materials are characterized with the ability to spontaneously transport water and other liquids. The wetting is driven by capillary forces that are induced by interfacial tension, that are stronger than the gravity force and viscous forces [3], [4]. This process occurs because of energy differences and thermodynamic will to achieve lower energy state [5]. The physics behind this phenomenon interested people from ancient time till our modern days but most of the theoretical background that I used in my report was researched and discovered during the 20<sup>th</sup> century.

### Capillary pressure and wicking dynamics

The wettability is the ability of a fluid phase to preferentially wet a solid surface in a presence of a second fluid phase [6]. In our case we have two phase fluid flow in a porous media. In this process we have 3 interfaces of interaction, two of them are fluid-solid and the other one is fluid-fluid. The wetting phase is a fluid-solid interface that has relatively smaller interfacial tension than the other a fluid-solid interface that called the non-wetting phase. Since interfacial tension has a direct relation to the interfacial energy, we can figure out that under isothermal conditions, the solid that which is filled with the wetting phase has higher energy compared to the same solid filled with wetting phase. That's the reason to the spontaneous imbibition of the wetting fluid as this system goes to a lower energy state. The imbibition will get stronger as the affinity between the fluid and the solid increase. This phenomenon correlates with the definition of capillary pressure and can be understood from it [4]. The capillary pressure is the pressure difference between two immiscible fluids in a thin tube [6]:

$$(1) \quad p_c = p_{nw} - p_w$$

Where:  $p_c$  is the capillary pressure,  $p_{nw}$  pressure in non-wetting phase,  $p_w$  pressure in wetting phase.

Also, the capillary pressure can be shown as:

$$(2) \quad p_c = \frac{2\gamma_{nw} \cdot \cos \theta}{r}$$

Where:  $p_c$  is the capillary pressure,  $\gamma_{nw}$  is the interfacial (surface) tension of the non-wetting phase,  $\theta$  is the contact angle and  $r$  is the radius of the thin tube.

Surface or interfacial tension is the cohesive force of molecules at the surface of an element attracting toward one another to take up the least possible surface area. In even simpler terms, it measures how much force it takes to keep a liquid together. Connection between surface tension of different interfaces can be described by Young's equation [5]:

$$(3) \quad \gamma_{sv} = \gamma_{sl} + \gamma_{lv} \cos(\theta)$$

Where:  $\gamma_{sv}$  is the surface tension in the solid-vapor (or solid-non-wetting) interface,  $\gamma_{sl}$  is the surface tension in the solid-liquid (or solid-wetting) interface,  $\gamma_{lv}$  is the surface tension in the liquid-vapor (or wetting-non-wetting) interface and  $\theta$  is the contact angle.

The contact angle is measured as the angle where a fluid interacts with a solid surface. A high contact angle ( $\theta > 90^\circ$ ) indicates that the surface has low wetting (in our words hydrophobic), A low contact angle ( $\theta < 90^\circ$ ) indicates that the surface is high wetting (in our case hydrophilic). A perfect wetting is achieved when the contact angle is 0, that means that all the liquid is absorbed by the solid.

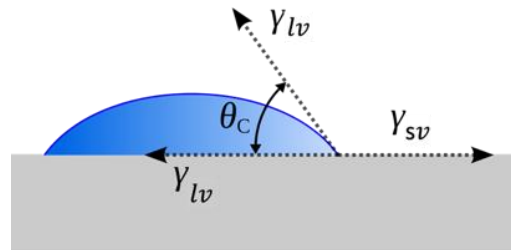


Figure 1: contact angle representation

As we can see in equation (3) the contact angle can be represented also via the different surface tensions. If we will combine equations (2) and (3) we can get this expression for surface pressure:

$$(4) \quad p_c = \frac{2(\gamma_{sv} - \gamma_{sl})}{2}$$

Where:  $\gamma_{sv}$  is the surface tension in the solid-vapor interface,  $\gamma_{sl}$  is the surface tension in the solid-liquid interface

Obviously, the bigger the difference between the interfacial tension (the bigger the affinity of the solid phase to the fluid phases difference), the larger the capillary pressure.

The contact angle must be determined also and Washburn in his works explained that in his works. The original Washburn's equation was used in describing of the capillary penetration of liquids [7]:

$$(5) \quad x^2 = \frac{R_{eff} \gamma_l \cos \theta}{2\eta} \cdot t$$

Where,  $R_{eff}$  is the effective radius of the interparticle capillaries,  $\gamma_l$  is the surface energy of the probe liquid,  $\eta$  is the liquid viscosity.

We can see that there is a linear connection between  $x^2$  and  $t$ . If we will know all the material constants, we can use the slope of these graph to find the contact angle  $\theta$ .

There is another common way of Washburn's equation [8]:

$$(6) \quad h^2 = \frac{cr\gamma_l \cos \theta}{2\eta} \cdot t$$

Where,  $h$  is the wetting height,  $r$  is the capillary radius,  $c$  tortuosity factor.

We can use the linear connection between  $h^2$  and  $t$  to calculate the contact angle  $\theta$ . Based on this equation and other that involve the contact angle, we have a big amount of contact angle determination methods[9]:

1. **The sessile drop** method: One of the most common methods that are used for determining the contact angle. In this method a droplet is placed on a solid sample and picture of it is taken by high-resolution camera. This photo is analyzed by the computer and the contact angle is calculated there.
2. **The Wilhelmy plate** method: This method is originally used for surface tension method but using young equation can be also implemented for contact angle measurements. The method involves a force tensiometer that is connected to a plate that is covered by water. The force is measured, then the surface tension is extracted from it and afterwards the contact angle is calculated.
3. **The Washburn** method: This method is the most popular method for powders and composite fibers. The method is based on capillary rise where the tested surface is pulled into water bath and a camera follows and document the ascent of the liquid in the sample or an electric scale measures the mass of the absorbed liquid. The curve that we receive during this method can be processed and the contact angle can be determined from it[10].

There are more techniques for contact angle determination that I haven't presented. Also, these methods can be used for surface energy determination. The Washburn method is the method that we used in our experiment, since we had almost a perfect complete wetting between the cellulose and the water.

### Multi component surface energy theories

There is different multi component surface energy theories that evolved with the years.

#### Fowkes approach [11]

Fowkes made a first term approximation in  $\gamma_{sl}$  that stands for the surface tension for the solid-liquid interface and rewrite it in this way, by derivation to 2 components polar (Hydrogen bonds) and dispersive component (van-der-Vaal's bonds):

$$(7) \quad \gamma_{sl} = \gamma_s^p + \gamma_s^d$$

where  $p$  refers to the polar component of the force and  $d$  refers to the dispersive component.

Using (7) we can rearrange the equation by rewriting some of its terms get another expression

for the surface energy:

$$(8) \quad \gamma_{sl} = \gamma_{sv} + \gamma_{lv} - 2\sqrt{\gamma_s^p \cdot \gamma_l^p} - 2\sqrt{\gamma_s^d \cdot \gamma_l^d}$$

If we continue with the derivations of the contact angle via our new polar and dispersive terms, we can get this equation:

$$(9) \quad 1 + \cos \theta = 2\sqrt{\gamma_s^d} \left( \frac{\sqrt{\gamma_l^d}}{\gamma_{lv}} \right) + 2\sqrt{\gamma_s^p} \left( \frac{\sqrt{\gamma_l^p}}{\gamma_{lv}} \right)$$

where  $p$  refers to the polar component of the force and  $d$  refers to the dispersive component.

Owens and Wendt model[12]

Owens and Wendt extended Fowkes approach and suggested a new method for describing surface tension between 2 surfaces. They introduce a fictional variable  $\gamma_c$  which can be described as:

$$(10) \quad \gamma_c = \gamma_s - \gamma_{sl}$$

With this definition we can express  $\gamma_c$  as:

$$(11) \quad \gamma_c = \gamma_s - \left[ \left( \sqrt{\gamma_s^d} - \sqrt{\gamma_l^d} \right)^2 - \left( \sqrt{\gamma_s^p} - \sqrt{\gamma_l^p} \right)^2 \right]$$

Where: The expression in the brackets is basically  $\gamma_{sl}$ .

From this equation (11) it is obvious that  $\gamma_s - \gamma_c$  is non-negative. And they were interested in 3 cases:

1. Non-polar liquid,  $\gamma_l^p = 0$ . Then  $\gamma_s^d = \gamma_l^d = \gamma_c$ .
2. Polar liquid on non-polar solid,  $\gamma_l^p \neq 0$  but  $\gamma_s^p = 0$ . Then  $\gamma_s = \gamma_s^d > \gamma_l^d$  and

$$\gamma_s - \gamma_c = \left( \sqrt{\gamma_s^d} - \sqrt{\gamma_l^d} \right)^2$$

3. Non-polar liquid on polar solid,  $\gamma_l^h = 0$  but  $\gamma_s^p \neq 0$ .

$$\text{Then } \gamma_s - \gamma_c = \left( \sqrt{\gamma_s^d} - \sqrt{\gamma_l^d} \right)^2 + \gamma_s^p.$$

van Oss model [13]

van Oss decided to treat the polar components as an acid-base components the apolar (dispersive) components remained van-der-Vaal's. The apolar interactions were described as:

$$(12) \quad \gamma_{ij}^{LW} = \gamma_i^{LW} + \gamma_j^{LW} - 2\sqrt{\gamma_i^{LW}\gamma_j^{LW}}$$

When: LW is a sign for van-der-Vaal's components.

The polar components can be described as:

$$(13) \quad \gamma_i^{AB} = 2\sqrt{\gamma_i^+\gamma_i^-}$$

When: AB stands for acid-base,  $\gamma_i^+$  is the electron donor and  $\gamma_i^-$  is the electron acceptor.

Then the total surface tension can be described as:

$$(14) \quad \gamma_i^{TOT} = \gamma_i^{LW} + \gamma_i^{AB}$$

Then the polar interaction can be described using:

$$(15) \quad \gamma_{ij}^{AB} = 2\left(\sqrt{\gamma_i^+\gamma_i^-} + \sqrt{\gamma_j^+\gamma_j^-} - \sqrt{\gamma_i^+\gamma_j^-} - \sqrt{\gamma_i^-\gamma_j^+}\right)$$

van Oss also showed us how to implement these definitions in Young's equation:

$$(16) \quad (1 + \cos \theta)\gamma_i^{TOT} = 2\left(\sqrt{\gamma_s^{LW}\gamma_i^{LW}} + \sqrt{\gamma_s^+\gamma_i^-} + \sqrt{\gamma_s^-\gamma_i^+}\right)$$

Now using (12) and (15) we can get the full interaction definition:

$$(17) \quad \gamma_{ij}^{TOT} = \left(\sqrt{\gamma_i^{LW}} - \sqrt{\gamma_j^{LW}}\right)^2 + 2\left(\sqrt{\gamma_i^+\gamma_i^-} + \sqrt{\gamma_j^+\gamma_j^-} - \sqrt{\gamma_i^+\gamma_j^-} - \sqrt{\gamma_i^-\gamma_j^+}\right)$$

### Capillary thermodynamics in fibrous materials

During the history the humankind widely used paper in everyday life. Nowadays with the technology progress we found new uses for paper. For example, paper-based microfluidics [14] and cardboard packages [15]. For these needs we must be able to control the wicking dynamics, to enhance or decline the wetting. For this purpose, many techniques were invented in the last years. For example, wax boundaries [16], [17], different shapes, special paper coatings [18]–[20] and plasma treatment [21]–[24]. Unfortunately, there are some fundamental problems that aren't well understood yet. For example, heat release. The wetting process of the water is accompanied with an interesting phenomenon which includes a temperature rise in the imbibition front [4]. There are some explanations to the temperature rise origin, one of the recent research papers in this field claims that it is due to acid-base and electrostatic interactions [3]. These phenomena can help us to follow the wetting front very easily and in a precise way with an IR camera and

get the imbibition height and velocity at every time step [25]. Also, the use of an IR camera can help us to understand the thermodynamics of the different wetting processes.

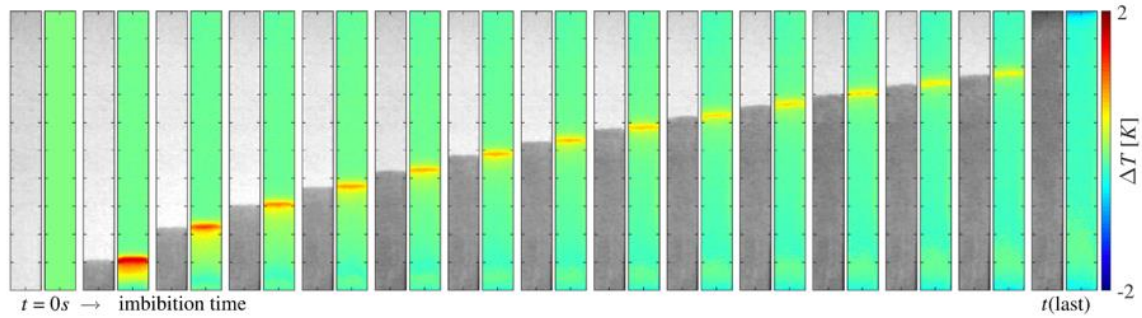


Figure 2: heat release demonstration in a paper sample filled with water from [26]

### Objective and goals

Plasma treatment of cellulose paper and other polymers is already in wide use. Some use this method to preserve an ancient writing from mold, bacteria, and wetting [24]. Others use it in the packaging industry [21], [23]. We already know that plasma affects wettability and adhesion of polymers [22]. In the research we were interested in the way that plasma treatment of a material surface can affect the wetting process both dynamics and thermodynamics. The results that will be obtained from this experimental study may help us to understand more clearly the influence and the fundamentals of the plasma treatment of paper-based materials.

## Materials and Methods

### Experimental system

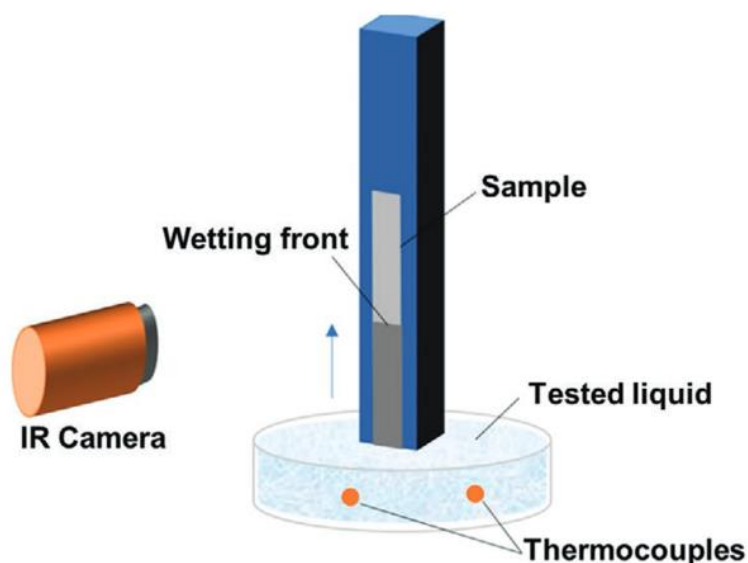


Figure 3: Experimental setup from [25]

The experimental setup is presented in Figure 3. The setup consists of an acrylic stand where the paper sample is installed, a constant temperature liquid bath and a thermal instrumentation (IR camera). The paper samples were made in  $3 \times 60$  (mm) and a  $6 \times 60$  (mm), that were cut in the same direction so that any influence of fiber orientation is the same for all experiments. In order to eliminate liquid evaporation from the wet paper surface, we covered the front side by a clear polypropylene tape of  $50 \mu\text{m}$  thickness that is also transparent to infrared radiation (transmittance 90%). Both edges of the paper-tape packing were carefully trimmed with a cutter in alignment with the acrylic stand. Hence, they were in contact with the atmosphere. The pressure above the wetting front during imbibition was therefore always ambient. The temperatures of the liquid bath, the plate sample and the surroundings were measured with thermocouples. The liquid bath was maintained at the same temperature with the paper (room temperature) in order to ensure that no heat is transferred from the bulk liquid to the cellulosic material (and vice versa). Once isothermal conditions were obtained, the liquid bath was touching the lower edge of the paper initialising imbibition against gravity. Optical and thermal images were then recorded to quantitatively visualise the liquid invasion process. The local temperature distribution was acquired by a FLIR-SC7000C IR camera ( $640 \times 512$ ). The IR camera were installed in such a distance from the paper sample providing a comparative field of view with a spatial resolution of about  $30 \text{ pixels}/(\text{mm})^2$ . Therefore, each pixel side corresponded to about  $0.1818 \text{ mm}$ . Both cameras were set at a constant frame rate of 4 Hz while

their temporal correlation was accomplished by removing an object of higher temperature in the monitoring frame before each experimental run. [25]

#### Sample material

The paper sample that was used in the experiment was 100% pure cellulose. When the chemical formula of cellulose is given:

$$(18) \quad (C_6H_{10}O_5)_n$$

Also, the chemical structure can be sketched as:

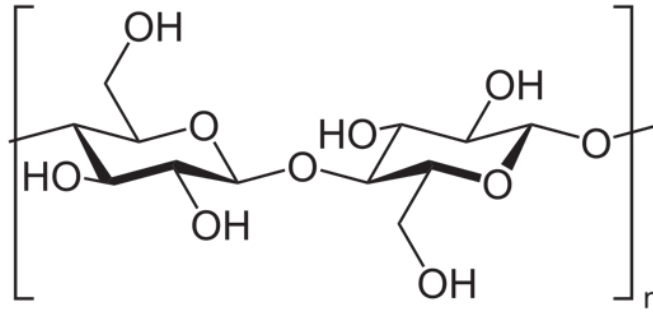


Figure 4: Chemical structure of cellulose

We performed an XRD (X-ray Diffraction Analysis) analysis on our paper sample, to prove the composition of our samples. The results of an untreated paper sample are:

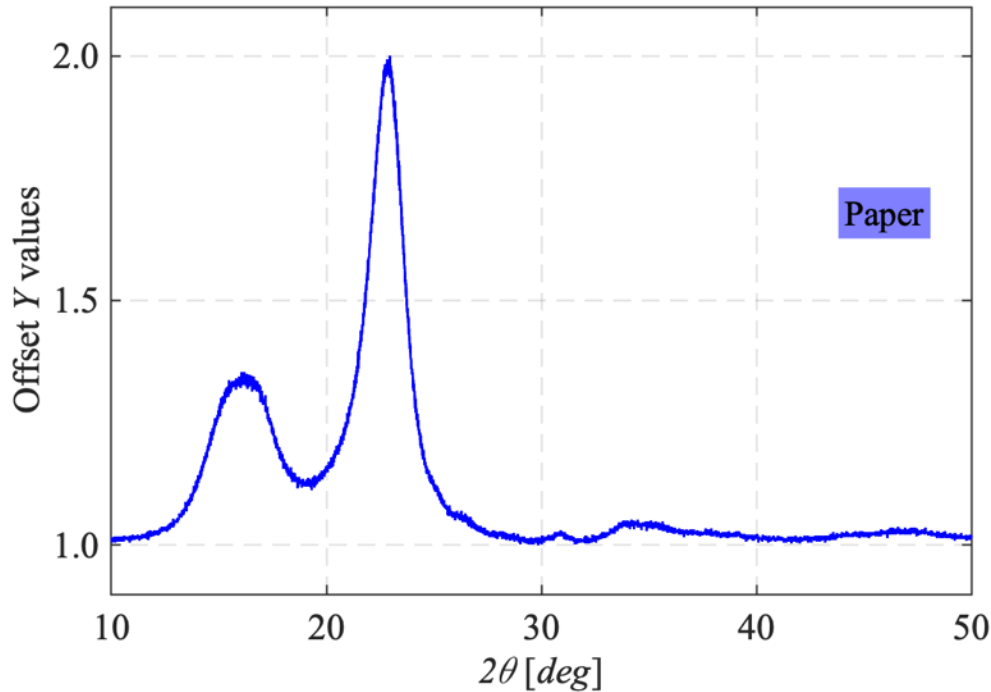


Figure 5: XRD analysis for paper sample

As we may notice, the values and the curve shape that we received is typical for a pure cellulose sample [27]. As our paper is made of pure cellulose that is a fibrous material the microstructure will involve fibers. These fibers can be noticeable in our SEM images that we took. When the

paper enters material, it fills the gaps between the fibers and bonds to the cellulose via hydrogen bonds.

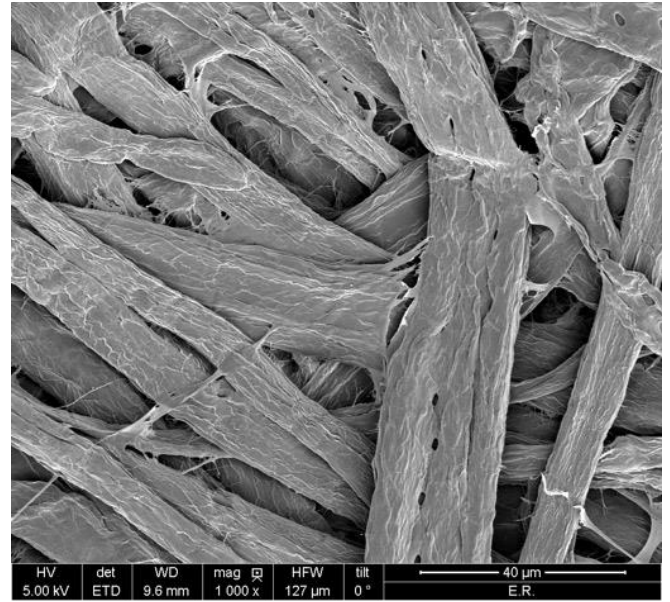
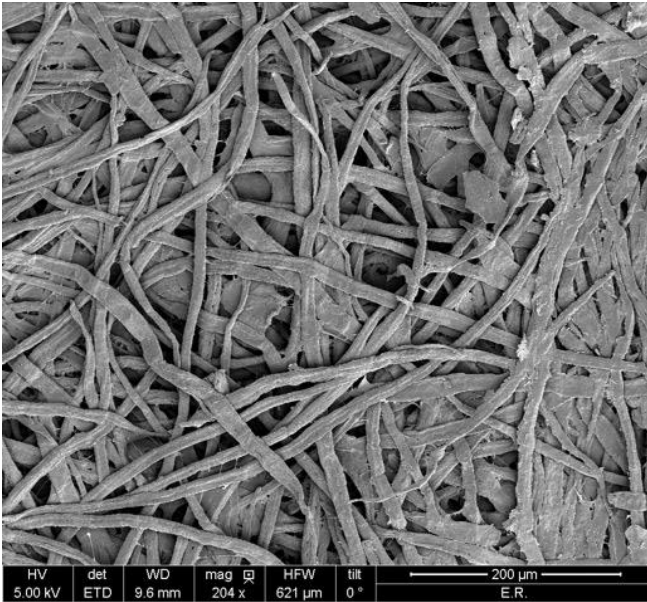


Figure 6: SEM top view pictures for the untreated paper sample

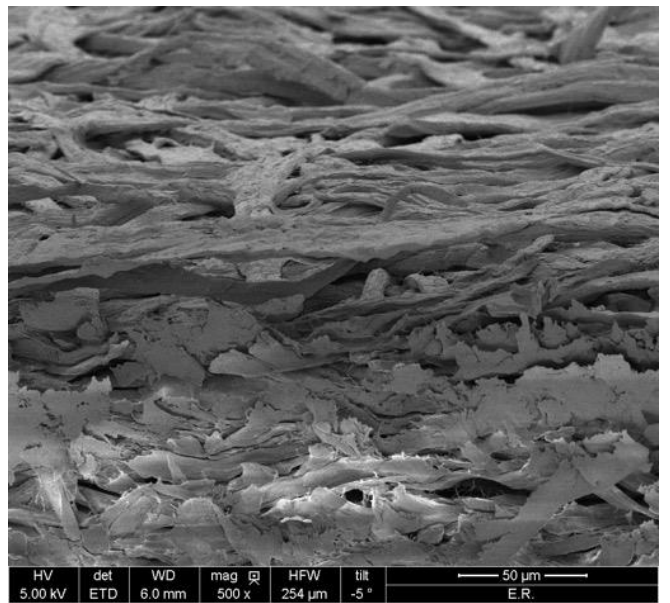
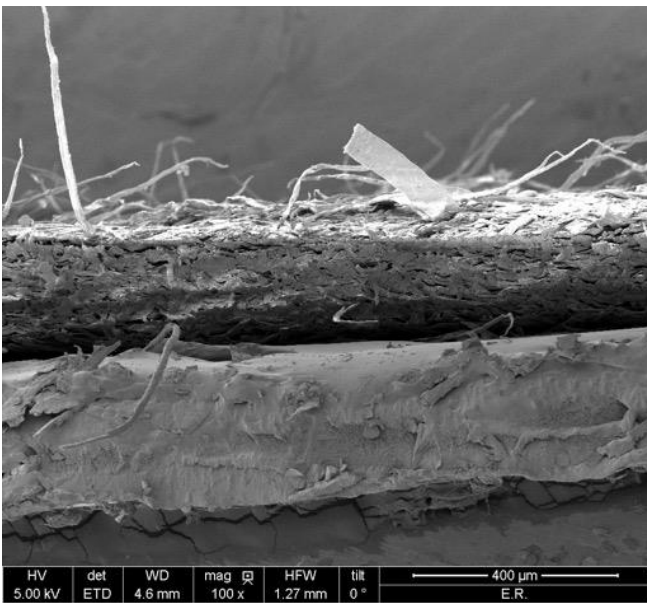


Figure 7: SEM side view pictures for the untreated paper sample

## Plasma treatment

The plasma treatment device that was chosen and used is “Diener Femto Plasma Etcher” by diener electronic. This device is a basic lab plasma coating machine, which is simple to use and maintain.



Figure 8: Plasma treatment system

The plasma creation mechanism is very complicated, but I'll try to explain it briefly and in a simple way. When neutral atoms that consists of negative electrons, positive protons and neutral neutrons that don't have a significant role in this process are put in a very high electric field, where electrons have enough energy to break the bonds to its nucleus and get "shot" from the atom creating a free electron that freely moves in the electric field and a positive ion. This electron can hit other atoms and ionize them also, so this process works like a chain reaction, every free electron hit other atoms and ionize them so other electrons break out of the atom and become free. During this process the collisions and the detachment of the electron involves a release of energy that is accompanied by a photon emission in different energy levels. These emittions create the glowing effect that we can see in our device. Then these ions can accelerate in the electric field and bombard the surface that is placed in the machine.

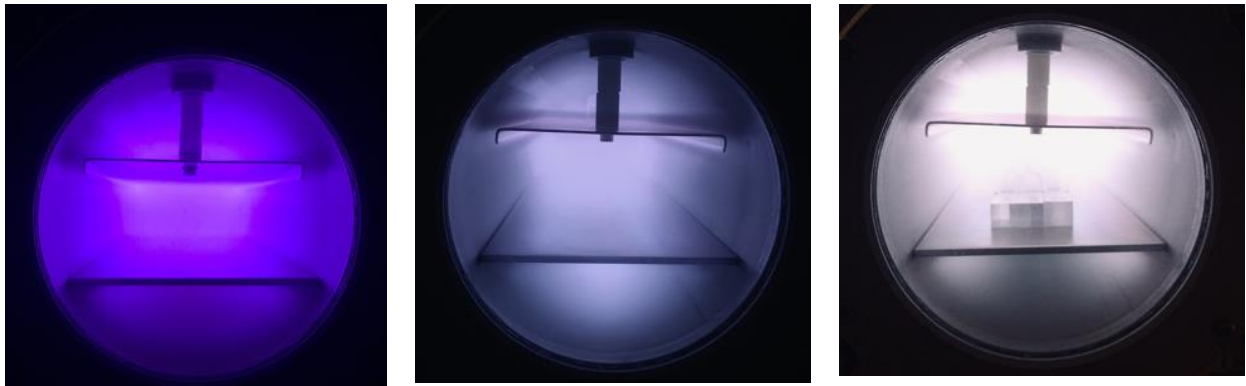


Figure 9: Plasma treatment process for Ambient air , Hydrogen and Oxygen plasmas

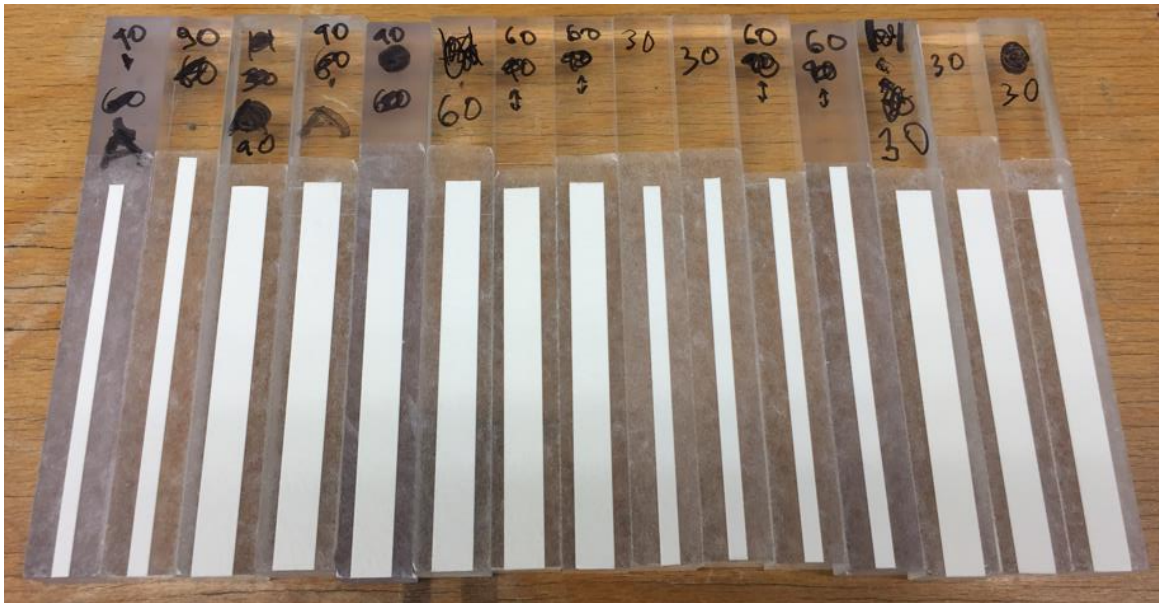


Figure 10: Paper samples that are used in the experiment



Figure 11: Paper sample putted in the plasma treatment machine

## FTIR spectroscopy analysis

To get a scientific explanation to the results that we got in our experiment, we performed FTIR spectroscopy analysis to our untreated, oxygen treated, and hydrogen treated paper samples. FTIR stands for “Fourier Transform InfraRed” and like any spectroscopy, this is a great tool for determination of functional groups in a test sample, together with possible molecular bonds between chemical composites. All the IR spectroscopies are based on the same phenomena – the IR radiation absorption by the different chemical bonds when the radiation passes through the sample. The FTIR spectroscopy is the most popular, fastest, and reliable method of spectroscopy. When an IR radiation passes through the sample a detector receives this radiation, processes it, and returns data about this radiation beam as an interferogram to the computer. When the computer uses Fourier transformation software and interprets the signal to an IR spectrum that can be read by us.[28]

The determination of the functional groups can be done due to IR absorption of different chemical bonds and the returned wavelength. Fortunately, we already know to what functional groups the wavelengths refer.

The wavenumber values that represent different functional groups can be found in different literature, we used [28], and the table that was given in pg. 7.

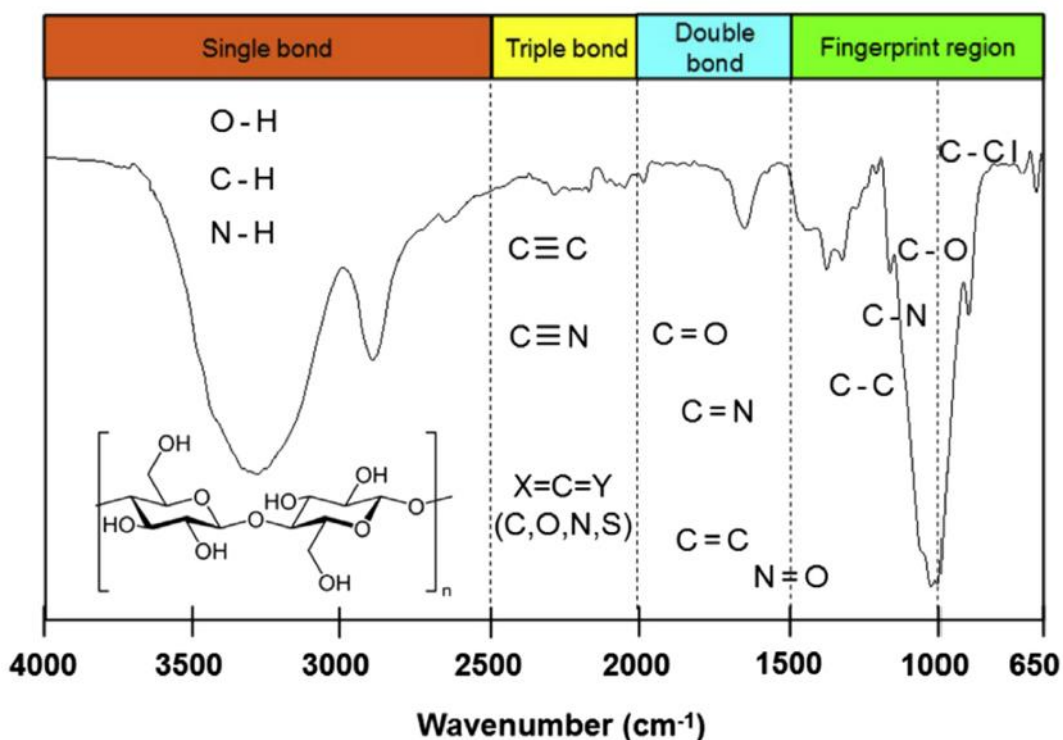


Figure 12: An example from [28] to an IR spectrum for a cellulose membrane

The values of the peaks that represent different functional groups can be extracted from it:

Peak Assignment	Peak Frequency ( $\text{cm}^{-1}$ )
O—H stretching	3336
C—H stretching	2895
O—H bending	1650
C—H <sub>2</sub> symmetric bending	1419
C—H bending	1369
C—H <sub>2</sub> wagging	1313
C—O antisymmetric stretching	1154
C—O and C—C stretching	1105
C—O and C—C stretching	1015
C—O—C stretching	891

Table 1: Fourier transform IR absorption band for functional group of regenerated cellulose membrane, from [28]

Our FTIR spectroscopy results are presented in the following figure:

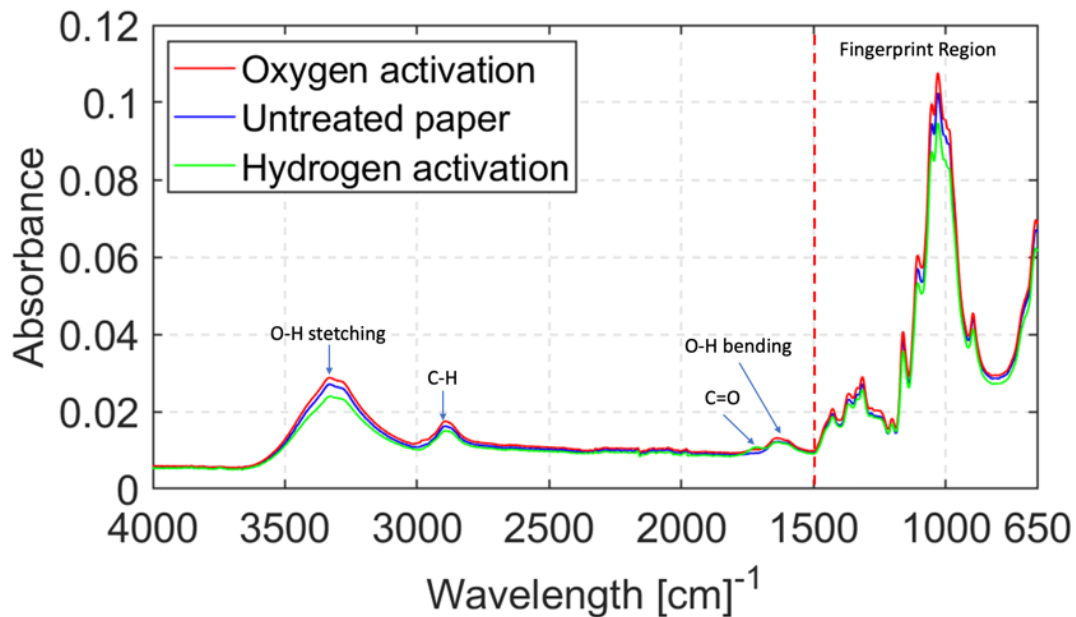


Figure 13: IR spectrum for 3 different treated paper samples (untreated, oxygen treated, hydrogen treated)

In the figure we can see all the 3 different samples that we had, superimpose on each other. We can clearly see that the oxygen activated paper sample has higher values of absorbance for all the functional groups except the  $C = O$  group. Higher values of absorbance mean that we have more presence of these groups the sample. We can clearly see that we have more hydroxyl groups ( $-OH$ ) in both types, bending and stretching. The hydroxyl groups have a critical role in wetting and the creation of hydrogen bonds between the cellulose molecules to the water molecules. Those hydroxyl compounds engage in intermolecular hydrogen bonding. As we know, the more hydroxyl compounds we have the more attractive is our material to water and it has more potential to create those hydrogen bonds with the water and get wet much quickly. From the given Figure 13 we can suppose that the oxygen treated paper sample will be more hydrophilic than the untreated sample when the hydrogen activated sample will be more hydrophilic than the untreated sample. The reason to these results will be described in the next chapter.

## Post-processing Program

To analyze and process the data we used MATLAB post processing program and routines that were modified to suit our data. Here I will explain about the functions we created and used.

**GetIRFrames** – A function that receive a file name of our IR data file (.asc) and returns to us the temperature value at every pixel of the given frame for each frame.

**ThermalPeakLocation** – a function that receive a matrix with the values of the temperature for each pixel and returns to us the Z location of the temperature peak.

**ImbibitionThresholdIR** – cuts the data that we have and makes the curve smother and cleaner and more accurate.

**ImbibitionCorrelation** – Calculates the imbibition speed  $\left(\frac{dz}{dt}\right)$  based on the IR correlation that we get from our data.

**ImDIP\_v1** is our main program. The abbreviation stands for Im(bibition) D(igital) I(mage) P(rocessing). This function can post process both CCD (.avi) and IR (.asc) experiment data files and return to us MATLAB data files for the curves that we presented in this work.

- First, we must choose the file that we want to post process.
- The program checks if our chosen filename has both (.avi) and (.asc) version before the start of the post processing. Based on this check the program can enter 2 branches of post processing for the CCD and for the IR data.
- Getting information of the materials used in the experiment for example, the liquid properties.
- Then we choose how much we want to crop the paper sample from the bottom.
- We get our data using GetIRFrames function.
- As we go ahead with the time steps, we get the imbibition height using ThermalPeakLocation.
- After that we start with the post processing of the imbibition curves, we clean and smooth our data signal using ImbibitionThresholdIR then we correlate the imbibition curve and calculate the material constant assuming complete wetting.
- When the program finishes this process, we can get our (.mat) file with the data.

## Results and Discussion

In this section I'll present the results that were obtained from our experiments, the influence of plasma on the both the dynamic and the thermodynamic phenomimes. Unfortunately, only part of our experiment was suitable for post processing and result presenting due to the fast imbibition reaction and bad recordings.

### Dynamic effect of plasma treatment

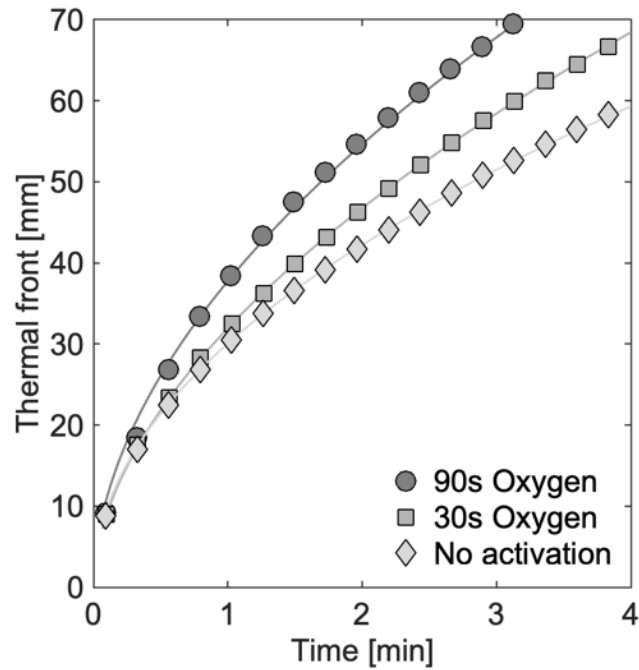


Figure 14: imbibition height vs time. for different types of plasma surface treatment for a 3mm paper sample

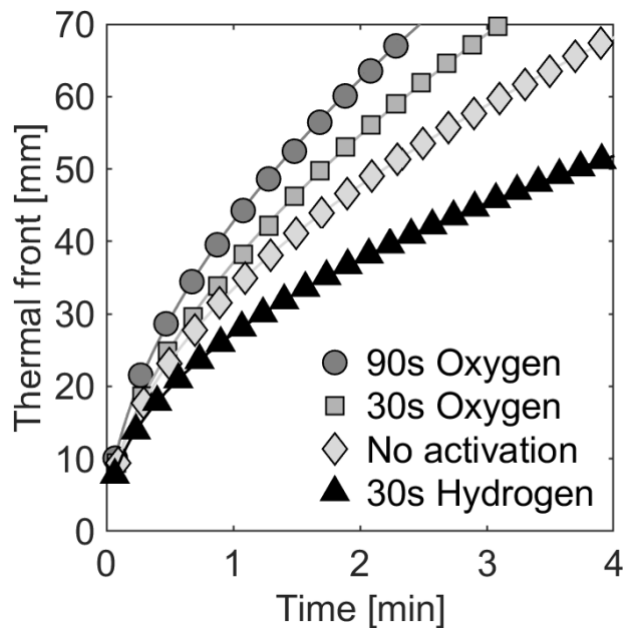


Figure 15: imbibition height vs time. for different types of plasma surface treatment for a 6mm paper sample

Figure 14 and Figure 15 give us the imbibition height as a function of time for different types of surface samples both plasma treated and untreated. We can clearly see the effect of the plasma treatment on the wettability of the surface. The oxygen plasma treatment accelerates the imbibition velocity when the hydrogen plasma does the opposite effect. Also, we can notice that longer exposure to the plasma during the treatment enhance the effect to both sides, faster imbibition with oxygen treatment vs slower imbibition with hydrogen treatment. Furthermore, larger area of the exposure will lead to a quicker wetting and bigger velocity of the thermal front. As was explained before we need hydrogen bonds to create connections between the cellulose and the water and wet the surface. From the FTIR we can see that oxygen plasma treated paper has more hydroxyls (OH- bonds) that can create more hydrogen bonds with the water, while in hydrogen plasma treated paper, we get a reduced amount of it. This fact was obtained and explained by Strom et al. in [29] while their conclusion was different. They got that both oxygen and hydrogen improve the wettability of the surface when we got that oxygen plasma improves it while hydrogen worsen it.

#### Thermodynamic effect of plasma treatment

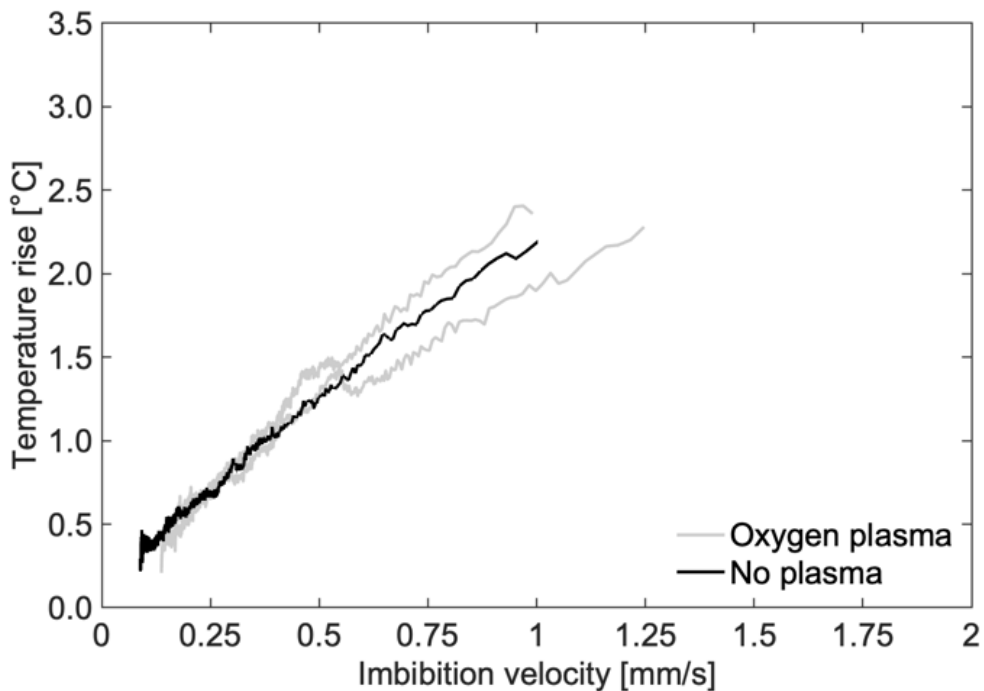


Figure 16: Temperature rise vs. Imbibition velocity for 3mm oxygen plasma treated and untreated paper

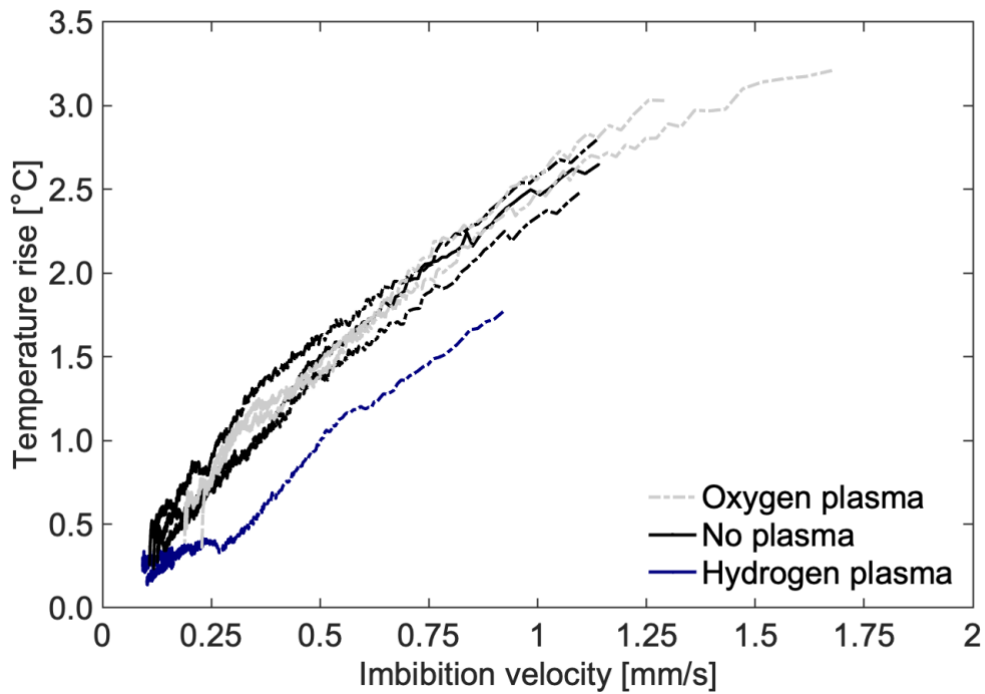


Figure 17: Temperature rise vs. Imbibition velocity for 6mm oxygen and hydrogen plasma treated and untreated paper

Figures 16-17 present the temperature rise at the wetting front as a function of the imbibition velocity. As was mentioned before water wetting of a pure cellulose is accompanied by an increase in temperature at the wetting front. As the water moving forward the velocity of the imbibition decrease as the temperature difference on the wetting front. We can see that temperature rise phenomenon can also be enhanced or diminished via plasma surface treatment. On Figure 17 we observe that hydrogen plasma treatment diminishes the temperature rise during the imbibition process, while oxygen plasma doesn't affect this as much as expected. Moreover, from Figure 16 we can confirm that the oxygen plasma doesn't affect the temperature rise that much. However, on Figures 14-15 we observed that oxygen plasma treatment increased the velocity of the imbibition during the whole imbibition process such that we can plot the temperature rise as a function of the imbibition height.

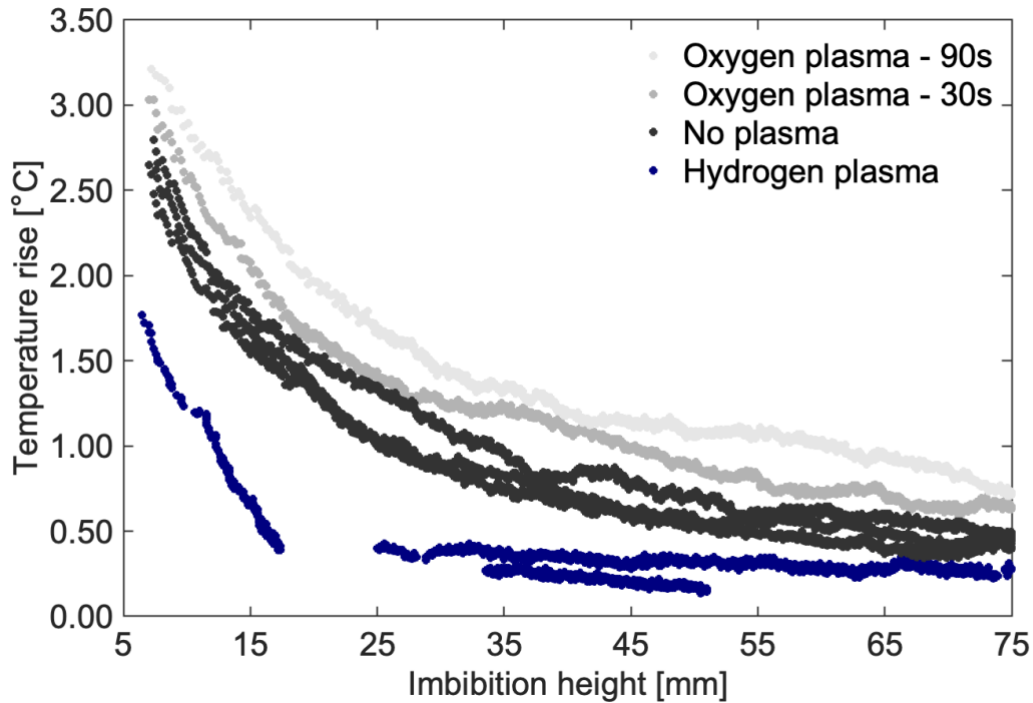


Figure 18: Temperature rise vs. Imbibition height for 6mm oxygen and hydrogen plasma treated and untreated paper

Figure 18 present the temperature rise of the wetting front as a function of the imbibition height. Here we can see the difference between oxygen, hydrogen plasma treated paper and untreated one. As we can observe oxygen plasma treatment increased the temperature rise on the wetting front while hydrogen plasma treatment decreased the temperature rise. As in the case of the enhancement of the imbibition velocity higher temperature were observed in the paper sample that was treated in the plasma machine for 90 seconds while the 30 seconds hasn't affected the temperature rise that much. We can notice that the hydrogen plasma treatment of the paper surface affected also the temperature rise at the wetting front and decreased it during the whole imbibition process.

#### Contact angle estimation

In this section I will estimate the different contact angles for the plasma treated surfaces. In previous experiments that was conducted by Terzis et al. for pentane where the contact angle of the water with the surface was approximately 0 ( $\cos\gamma \approx 1$ ) the coefficient  $K = \frac{R_{eff}}{2}$  was estimated - Figure 19. Using (5) and the water properties we can calculate the contact angles.

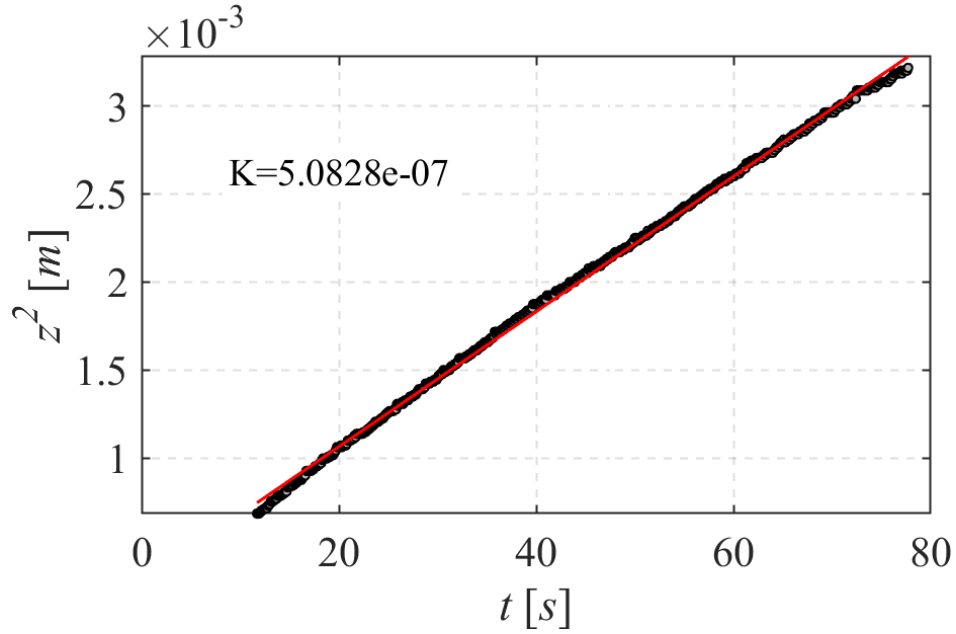


Figure 19:  $z^2$  as a function of  $t$  with the approximated slope for an experiment of pentane with untreated paper sample

The known properties of the water are:  $\gamma = 71.94 \left[ \frac{mN}{m} \right]$  ,  $\eta = 0.89 \left[ \frac{mPa}{s} \right]$

when  $\frac{R_{eff}}{2} = 5.0828 \times 10^{-7}$  . Approximations were made to get a proper slope for the equations.

The contact angle can be evaluated using:

$$(19) \quad z^2 \cdot \frac{2\eta}{R_{eff}\gamma_l t} = \cos \theta$$

The estimated contact angles are:

Paper sample	contact angle – $\theta$
Oxygen Treated For 90 [sec]	32.9°
Oxygen Treated Paper For 30 [sec]	47.7°
Untreated Paper	64.2°
Hydrogen Treated Paper For 30 [sec]	74.9°

Table 2: Estimated contact angles for different paper samples at 6 [mm]

As we can see from the tables, both oxygen and hydrogen treatments affected the contact angle as expected. Oxygen treatment reduced it (made the surface more hydrophilic) for a 90 sec treatment the contact angle reduced by 31.3°, for 30 sec treatment the reduction was 16.5° while hydrogen treatment increased the contact angle (made the surface more hydrophobic) by 10.7°.

An explanation to the results that we obtained can be found on Figure 13. We can notice that oxygen treated paper sample has a bigger amount of hydroxyl groups (OH- bonds) in reference to the untreated paper sample while the hydrogen sample has a smaller amount of this functional group. The presence of a larger number of hydroxyls gives the cellulose more junctions for hydrogen bonds so water propagates faster, and we have a larger amount of energy release at the wetting front. As presented on Figure 20 the higher the number of hydroxyls we have the larger amount of hydrogen bonds will be created and a higher amount of energy will release.

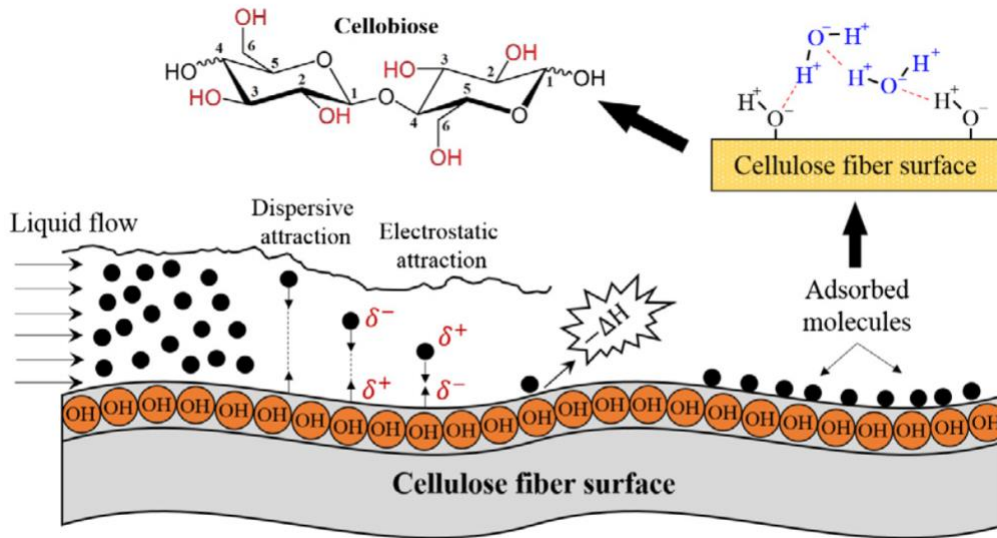


Figure 20: A schematic representation of the molecular interactions between cellulose and imbibed water from [26]

## Conclusion

The presented results gave to us a much brighter picture on the effects of plasma treatment of a paper surface. We observed that oxygen plasma treatment enhances the imbibition velocity and the temperature rise at the wetting front while hydrogen plasma treatment diminishes the velocity and the temperature rise. The contact angle is also affected by the treatment, when oxygen treatment decreases the contact angle and hydrogen treatment increase it. Also, we noticed that that the higher the exposure of the paper sample to the plasma treatment processes the higher the effect of this treatment. The results that we received was different from the most popular research on this topic [30]. Strom et al. received that both oxygen and hydrogen plasma treatments enhance the wetting procedure while we received that only oxygen plasma treatment enchases these phenomes while the hydrogen plasma treatment does the opposite effect. A possible explanation to these effects can be found using FTIR spectroscopy of the paper samples and then the comparison between them. We found that the oxygen plasma treated paper have a larger number of hydroxyl groups (OH- bonds) in the paper surface then untreated paper sample while the hydrogen plasma treated paper sample has a smaller amount of these groups. Further experiment and research can be done on this topic. Different liquids, plasma treatment types, surface materials can be used in the imbibition process. Longer plasma treatment exposures amd a bigger amount of experiments can be performed.

## Bibliography

- [1] S. Nishat, A. T. Jafry, A. W. Martinez, and F. R. Awan, "Paper-based microfluidics: Simplified fabrication and assay methods," *Sens Actuators B Chem*, vol. 336, Jun. 2021, doi: 10.1016/j.snb.2021.129681.
- [2] A. W. Martinez, S. T. Phillips, G. M. Whitesides, and E. Carrilho, "Diagnostics for the developing world: Microfluidic paper-based analytical devices," *Anal Chem*, vol. 82, no. 1, pp. 3–10, 2010, doi: 10.1021/ac9013989.
- [3] A. Terzis *et al.*, "Heat release at the wetting front during capillary filling of cellulosic micro-substrates," *J Colloid Interface Sci*, vol. 504, pp. 751–757, Oct. 2017, doi: 10.1016/j.jcis.2017.06.027.
- [4] H. Aslannejad, A. Terzis, S. M. Hassanizadeh, and B. Weigand, "Occurrence of temperature spikes at a wetting front during spontaneous imbibition," *Sci Rep*, vol. 7, no. 1, p. 7268, Dec. 2017, doi: 10.1038/s41598-017-07528-7.
- [5] R. J. Good, "Contact Angle, Wetting, and Adhesion: A Critical Review," *J Adhes Sci Technol*, vol. 6, no. 12, pp. 1269–1302, Jan. 1992, doi: 10.1163/156856192X00629.
- [6] J. R. Fanchi, *Shared Earth Modeling*. 2002.
- [7] Edward Washburn, "The dynamics of a capillary flow," Illinois, 1921.
- [8] L. Ji and B. Shi, "A novel method for determining surface free energy of powders using Washburn's equation without calculating capillary factor and contact angle," *Powder Technol*, vol. 271, pp. 88–92, Feb. 2015, doi: 10.1016/j.powtec.2014.11.002.
- [9] A. Alghunaim, S. Kirdponpattara, and B. M. Z. Newby, "Techniques for determining contact angle and wettability of powders," *Powder Technology*, vol. 287. Elsevier, pp. 201–215, Jan. 01, 2016. doi: 10.1016/j.powtec.2015.10.002.
- [10] L. Galet, S. Patry, and J. Dodds, "Determination of the wettability of powders by the Washburn capillary rise method with bed preparation by a centrifugal packing technique," *J Colloid Interface Sci*, vol. 346, no. 2, pp. 470–475, Jun. 2010, doi: 10.1016/j.jcis.2010.02.051.
- [11] F. M. Fowkes, "Attractive Forces At Interfaces," *Ind Eng Chem*, vol. 56, no. 12, pp. 40–52, Dec. 1964, doi: 10.1021/ie506660a008.
- [12] D. K. Owens and R. C. Wendt, "Estimation of the surface free energy of polymers," *J Appl Polym Sci*, vol. 13, no. 8, pp. 1741–1747, 1969, doi: 10.1002/app.1969.070130815.
- [13] C. J. van Oss, R. J. Good, and K. Chaudhury, "Additive and Nonadditive Surface Tension Components and the Interpretation of Contact Angles." [Online]. Available: <https://pubs.acs.org/sharingguidelines>
- [14] A. Sinha, M. Basu, and P. Chandna, "Paper based microfluidics: A forecast toward the most affordable and rapid point-of-care devices," in *Progress in Molecular Biology and Translational Science*, vol. 186, no. 1, Elsevier B.V., 2022, pp. 109–158. doi: 10.1016/bs.pmbts.2021.07.010.

- [15] M. S. Alamri *et al.*, “Food packaging’s materials: A food safety perspective,” *Saudi Journal of Biological Sciences*, vol. 28, no. 8. Elsevier B.V., pp. 4490–4499, Aug. 01, 2021. doi: 10.1016/j.sjbs.2021.04.047.
- [16] M. Boodaghi and A. Shamloo, “Effects of wax boundaries in combination with evaporation on dynamics of fluid flow in paper-based devices,” *Surfaces and Interfaces*, vol. 21, p. 100684, Dec. 2020, doi: 10.1016/j.surfin.2020.100684.
- [17] S. Hong and W. Kim, “Dynamics of water imbibition through paper channels with wax boundaries,” *Microfluid Nanofluidics*, vol. 19, no. 4, pp. 845–853, Oct. 2015, doi: 10.1007/s10404-015-1611-3.
- [18] S. M. Fadel, W. S. Abou-Elseoud, E. A. Hassan, S. Ibrahim, and M. L. Hassan, “Use of sugar beet cellulose nanofibers for paper coating,” *Ind Crops Prod*, vol. 180, Jun. 2022, doi: 10.1016/j.indcrop.2022.114787.
- [19] R. Shorey and T. H. Mekonnen, “Sustainable paper coating with enhanced barrier properties based on esterified lignin and PBAT blend,” *Int J Biol Macromol*, vol. 209, pp. 472–484, Jun. 2022, doi: 10.1016/j.ijbiomac.2022.04.037.
- [20] M. Huang, Y. Tang, X. Wang, P. Zhu, T. Chen, and Y. Zhou, “Preparation of polyaniline/cellulose nanocrystal composite and its application in surface coating of cellulosic paper,” *Prog Org Coat*, vol. 159, Oct. 2021, doi: 10.1016/j.porgcoat.2021.106452.
- [21] J. Gordon, “The Application of Plasma Technology in Packaging,” 2008.
- [22] R. Wolf and A. C. Sparavigna, “Role of Plasma Surface Treatments on Wetting and Adhesion,” *Engineering*, vol. 02, no. 06, pp. 397–402, 2010, doi: 10.4236/eng.2010.26052.
- [23] D. Skácelová, D. Kováčik, T. Homola, J. Čech, and M. Černák, “SURFACE MODIFICATION OF PAPER AND PAPERBOARDS USING ATMOSPHERIC PRESSURE PLASMAS.”
- [24] U. Vohrer, I. Trick, J. Bernhardt, C. Oehr, and H. Brunner, “Plasma treatment an increasing technology for paper restoration?,” 2001.
- [25] A. Terzis *et al.*, “A temperature-based diagnostic approach for paper-based microfluidics,” *Microfluid Nanofluidics*, vol. 22, no. 3, p. 35, Mar. 2018, doi: 10.1007/s10404-018-2054-4.
- [26] A. Terzis *et al.*, “Heat release at the wetting front during capillary filling of cellulosic micro-substrates,” *J Colloid Interface Sci*, vol. 504, pp. 751–757, Oct. 2017, doi: 10.1016/j.jcis.2017.06.027.
- [27] G. SriBala, R. Chennuru, S. Mahapatra, and R. Vinu, “Effect of alkaline ultrasonic pretreatment on crystalline morphology and enzymatic hydrolysis of cellulose,” *Cellulose*, vol. 23, no. 3, pp. 1725–1740, Jun. 2016, doi: 10.1007/s10570-016-0893-2.
- [28] N. Hilal, A. F. Ismail, T. Matsuura, and D. Oatley-Radcliffe, *Membrane characterization*. 2017.

- [29] G. Ström and G. Carlsson, "Wettability of kraft pulps—effect of surface composition and oxygen plasma treatment," *J Adhes Sci Technol*, vol. 6, no. 6, pp. 703–718, 1992, doi: 10.1163/156856192X01088.
- [30] G. R. Strom and G. Carlsson, "Reduction and oxidation of cellulose surfaces by means of cold plasma," *Polymeric Materials Science and Engineering, Proceedings of the ACS Division of Polymeric Materials Science and Engineering*, vol. 62, no. 9, p. 942, 1990.